Electronic Supplementary Material (ESI) for Journal of Materials Chemistry A.

Supporting information

Metastable oxysulfide surface formation on $LiNi_{0.5}Mn_{1.5}O_4$ single crystal particles by using carbothermal reaction with Sulfur-doped hetercarbon nanoparticles: New insight for their structural and electrochemical characteristics, and their potential applications

Dae-wook Kim[a] Nobuyuki Zettsu[a,b,*], Hiromasa Shiiba[b], Gabriel Sánchez-Santolino[c], Ryo Ishikawa [c,d], Yuichi Ikuhara[c], and Katsuya Teshima[a,b,*]

[a] Department of Materials Chemistry, Shinshu University, 4-17-1 Wakasato, Nagano, 380-8553, Japan
[b] Research Initiative for Supra-Materials, Shinshu University, 4-17-1 Wakasato, Nagano, 380-8553, Japan
[c] Institute of Engineering Innovation, The University of Tokyo, Tokyo, 113-8656, Japan
[d] Japan Science and Technology Agency, PRESTO, Kawaguchi, Saitama 332-0012, Japan

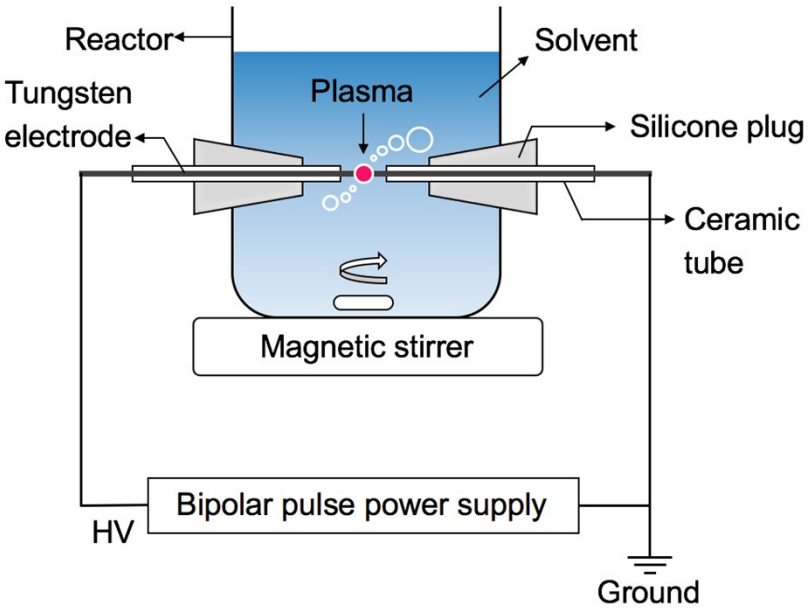

Fig. S1. Schematic illustration of reactor for solution plasma process (SPP). Sulfur doped amorphous hydrocarbon (S-HC) powders were synthesized by SPP. Nonequilibrium cold plasma in aromatic solvent resulted in the formation of amorphous nanocarbon powder having disordered phase. A thiophene (C_4H_4S) was used as a precursor in this study. A bipolar pulsed generator was used as a power supply for making glow discharge in thiophen. The applied voltage and pulse width were 1.6 kV and 2 μs, respectively.

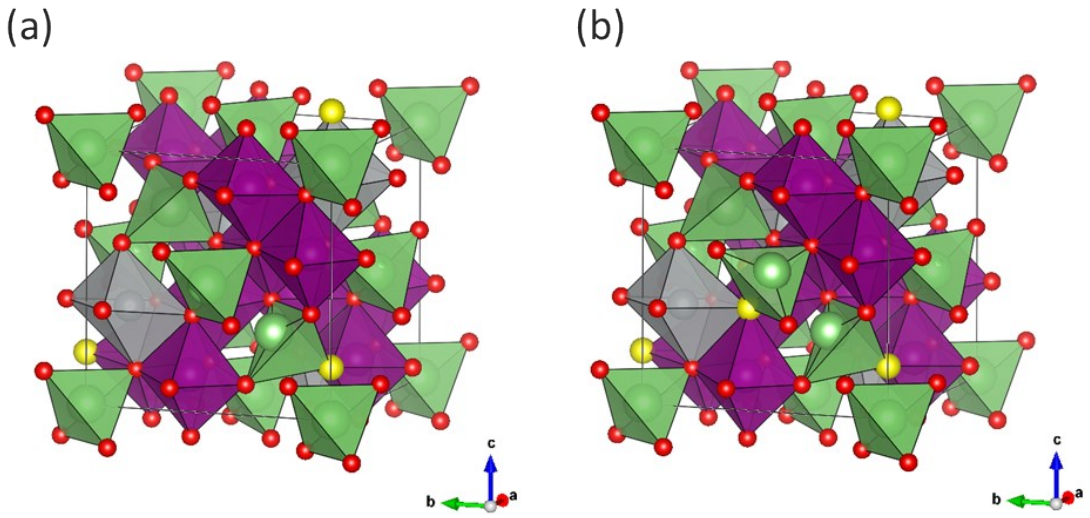

	O_4	$O_{3.875}S_{0.125}$	$O_{3.75}S_{0.25}$
a [Å]	8.178	8.220	8.258
b [Å]	-	8.242	8.284
c [Å]	-	8.213	8.272
Volume [Å^3]	546.96	556.47	565.88

Fig. S2. All possible O/S arrangements were considered to determine the most stable 2, and 13 different O/S arrangements, which were calculated by DFT calculation for x = 0.125, and 0.25, respectively: (a) x = 0.125, and (b) x = 0.25 in $LiNi_{0.5}Mn_{1.5}O_{4-x}S_x$ with $P4_332$ symmetry.

Table S1. The S^{2-} defect formation energy in $LiNi_{0.5}Mn_{1.5}O_{4-x}S_x$ for (a) x = 0.125 ($Li_8Ni_4Mn_{12}O_{31}S_1$), and (b) x = 0.25 ($Li_8Ni_4Mn_{12}O_{30}S_2$) were analyzed by DFT calculation. Each atom in $P4_332$ LNMO occupies $\{(Li)^{8c}\}_{tet}\{(Ni_{0.5})^{4b}(Mn_{1.5})^{12d}\}_{oct}(O)^{8c}(O_{3-x})^{24e}(S_x)^{24e}$, where superscripts indicate Wyckoff notation, and subscripts tet and oct indicate tetrahedral and octahedral sites, respectively. Sulfur defect formation energies, E^F, were calculated for two sulfur-deficient compositions, x = 0.125, 0.25.

(a)

	E^F (eV)
$8LiNi_{0.5}Mn_{1.5}O_{3.875}S_{0.125} \rightarrow 8LiNi_{0.5}Mn_{1.5}O_{3.875} + \frac{1}{8}S_8$	-0.20
$8Ni_{0.5}Mn_{1.5}O_{3.875}S_{0.125} \rightarrow 8Ni_{0.5}Mn_{1.5}O_{3.875} + \frac{1}{8}S_8$	0.37

(b)

	E^F (eV)
$8LiNi_{0.5}Mn_{1.5}O_{3.75}S_{0.25} \rightarrow 8LiNi_{0.5}Mn_{1.5}O_{3.75}S_{0.125} + \frac{1}{8}S_8$	-0.15
$8LiNi_{0.5}Mn_{1.5}O_{3.75}S_{0.125} \rightarrow 8LiNi_{0.5}Mn_{1.5}O_{3.75} + \frac{1}{8}S_8$	-0.11
$8Ni_{0.5}Mn_{1.5}O_{3.75}S_{0.25} \rightarrow 8Ni_{0.5}Mn_{1.5}O_{3.75}S_{0.125} + \frac{1}{8}S_8$	0.39
$8Ni_{0.5}Mn_{1.5}O_{3.75}S_{0.125} \rightarrow 8Ni_{0.5}Mn_{1.5}O_{3.75} + \frac{1}{8}S_8$	0.32

Formation of a single sulfur defect for x = 0.125 can be described by Kröger−Vink notation as

$$S_O^{\times} \rightarrow V_O^{\cdot\cdot} + 2e' + S \quad (1)$$

Formation of a single sulfur defect for x = 0.25 was considered as two-stage reactions as follows,

$$2S_O^{\times} \rightarrow S_O^{\times} + V_O^{\cdot\cdot} + 2e' + S \quad (2)$$

$$S_O^{\times} + V_O^{\cdot\cdot} \rightarrow 2V_O^{\cdot\cdot} + 2e' + S \quad (3)$$

E^F for equation (1 – 3) can be described as

$$E^F = 8E(LiNi_{0.5}Mn_{1.5}O_{3.875}) - 8E(LiNi_{0.5}Mn_{1.5}O_{3.875}S_{0.125}) + E(S) \quad (4)$$

$$E^F = 8E(LiNi_{0.5}Mn_{1.5}O_{3.75}S_{0.125}) - 8E(LiNi_{0.5}Mn_{1.5}O_{3.75}S_{0.25}) + E(S) \quad (5)$$

$$E^F = 8E(LiNi_{0.5}Mn_{1.5}O_{3.75}) - 8E(LiNi_{0.5}Mn_{1.5}O_{3.75}S_{0.125}) + E(S) \quad (6)$$

E(X) indicates total

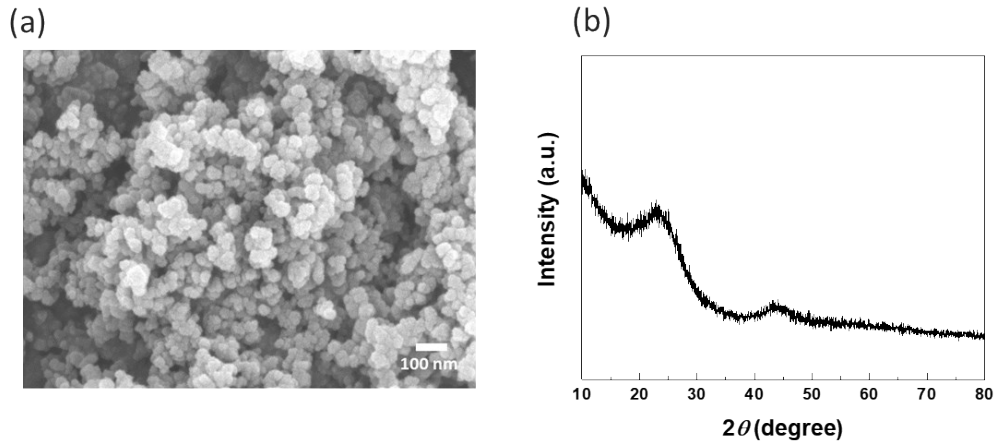

Fig. S3. Typical (a) FE-SEM image and (b) XRD profile of as synthesized S-HC powders.

Table S2. The chemical compositions of the $LiNi_{0.5}Mn_{1.5}O_{4-x}S_x$ crystals, evaluated by ICP-OES and XPS for cation and anion spices, respectively.

	ICP			XPS	
	Li	Mn	Ni	O	S
$LiNi_{0.5}Mn_{1.5}O_{3.90}S_{0.10}$ ($LNMOS_{0.1}$)	0.95	1.50	0.48	3.90	0.1
$LiNi_{0.5}Mn_{1.5}O_{3.85}S_{0.15}$ ($LNMOS_{0.15}$)	0.96	1.50	0.48	3.85	0.15

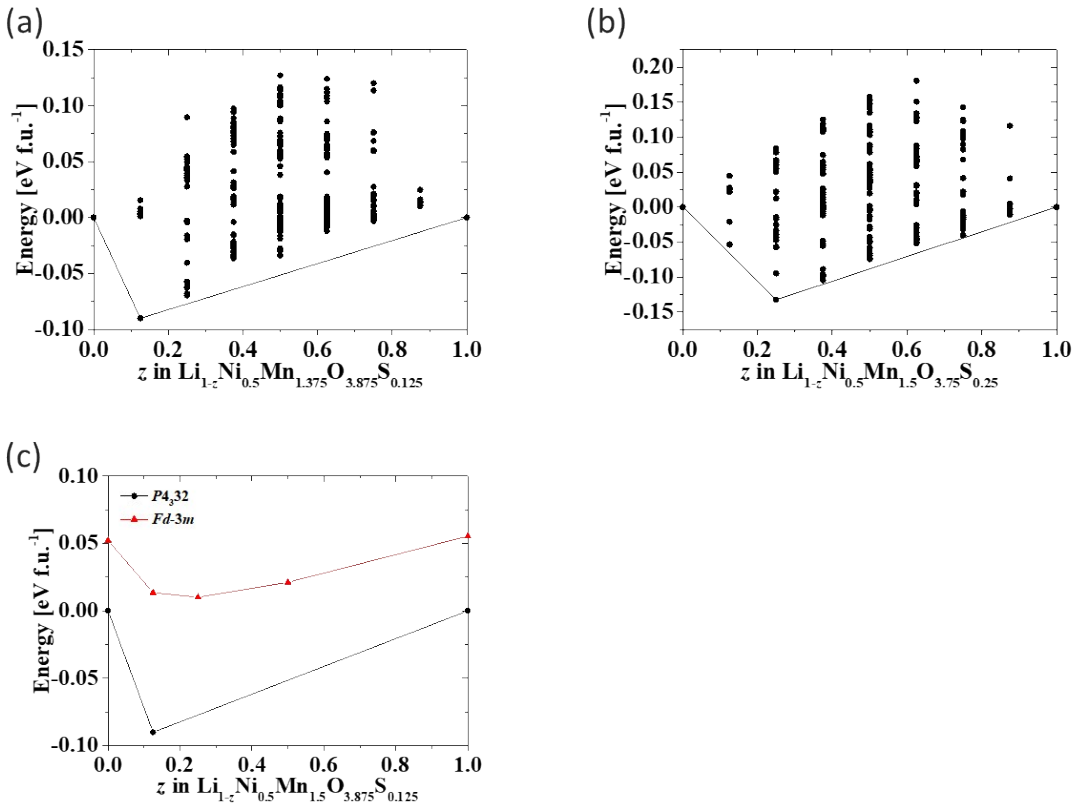

Fig. S4. The formation energies as a function of lithium composition in DFT-modeling $LNMOS_x$ frameworks (x = 0.125, and 0.25) with $P4_332$ symmetries. Electrochemical delithiation in spinel systems is believed to occur via both solid-solution and two-phase reaction mechanisms.

We evaluated formation energies of the all possible atomic arrangements for each LNMOS with different Li compositions. These figures plotted vertically the formation energies of the all possible atomic arrangements in each composition. Thus, the bottom one aligned on the y axis means the minimum formation energy, and its atomic arrangement will be the most plausible candidate as thermodynamically stable. I am going to explain the interpretation of the x-axis. This figure discusses the stability of the formation energy of the delithiated compositions based on the formation energy through comparing of the most stable atomic arrangement that is fully lithiated composition. Most important issue is that the all minimum formation energies in the delithiated compositions are positioned negative, indicating that delithiation reaction can progress via thermodynamics point of view. Furthermore, these figures strongly suggest a plausible reaction mechanism in the delithiation reaction. For instance, the energy of Li1-0.125NMOS0.125 showed negative value as comparing to that of fully lithiated Li1NMOS0.125. However, each formation energies in $Li_{1-x}NMOS_{0.125}$ ($0.25<x<0.875$) showed higher than the straight line joining point of $Li_{1-0.125}NMOS_{0.125}$ and $Li_0NMOS_{0.125}$. These characteristics implied that electrochemical lithiation reaction will progress under solid-solution reaction mechanism from $Li_1NMOS_{0.125}$ to $Li_{1-0.125}NMOS_{0.125}$ and will progress under two-phase reaction from $Li_{1-0.125}NMOS_{0.125}$ to $Li_{1-0.125}NMOS_{0.125}$.

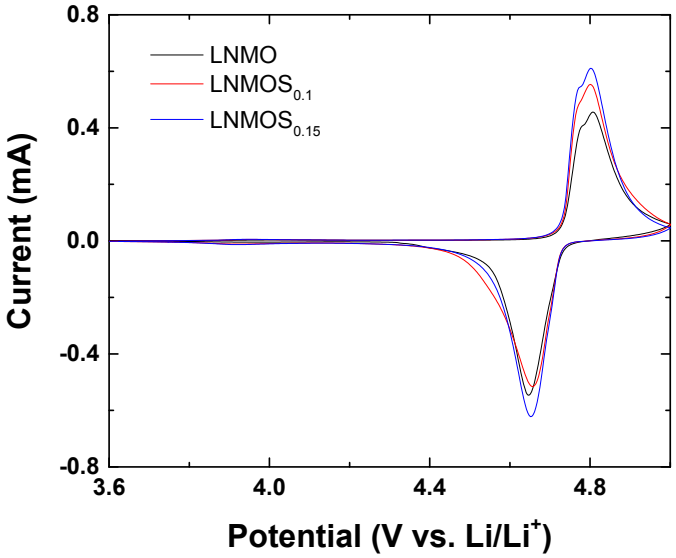

Fig. S5. Cyclic voltammograms of the LNMO/Li, and LNMOS$_x$/Li half cells with a scan rate of 0.15 mV/s.

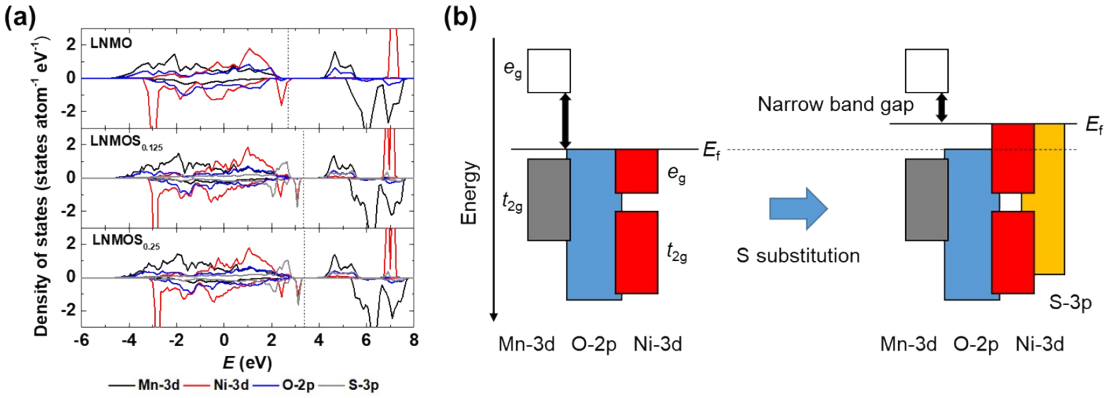

Fig. S6. (a) Orbital electronic structures of Mn-3d, Ni-3d, O-2p, and S-3p in some MO6/ MO5S octahedrons in LNMOSx. The value on the x-axis was set to the vacuum level. (b) Schematic diagrams summarizing the PDOS near Fermi level.

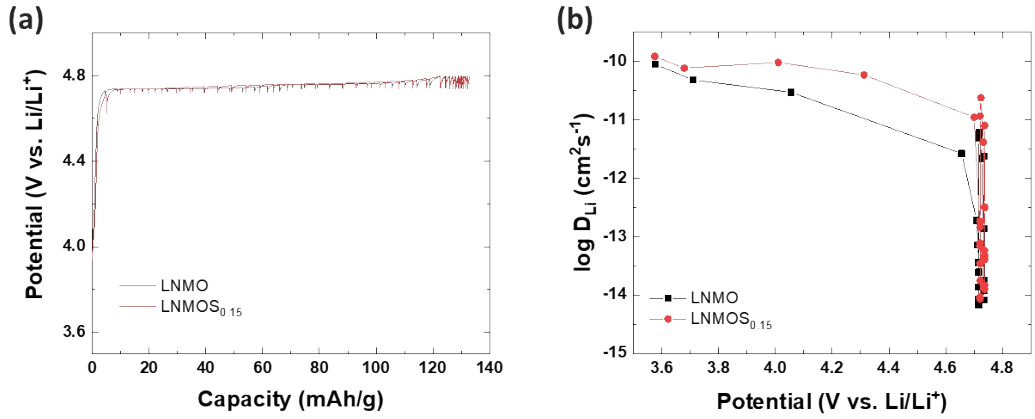

Fig. S7. (a) The galvanostatic intermittent titration technique (GITT) was performed at 0.2C for LNMO /Li and $LNMOS_{0.15}$/Li cell, respectively. Both cells were charged for 10 min and then followed by a relaxation time of 60 min between 3.5 and 4.8 V (vs Li/Li^+). (b) The changes in the Li^+ diffusion coefficient (D_{Li}) of LNMO and $LNMOS_{0.15}$ electrodes as a function of the presented voltage ranges. The D_{Li} of both electrodes revealed similar trend, which were relatively high Li^+ diffusivity up to 4.6 V (LNMO: 10^{-10}–10^{-11} cm^2s^{-1}, $LNMOS_{0.15}$: 10^{-9}–10^{-10} cm^2s^{-1}).

Table S3. Kinetic parameters of the LNMO/Li, and series of $LNMOS_x$/Li half cells after initial three cycles with C rate of 0.2 C and following 200 cycles with C rate of 1C.

	After 3 cycles			After 200 cycles		
	R_{sf}	R_{ct}	D_{Li}	R_{sf}	R_{ct}	D_{Li}
LNMO	8.67	8.74	8.47×10^{-12}	25.48	22.97	1.58×10^{-12}
$LNMOS_{0.1}$	8.95	5.92	1.04×10^{-11}	12.56	9.06	8.19×10^{-12}
$LNMOS_{0.15}$	12.04	6.01	8.03×10^{-12}	12.64	6.84	1.20×10^{-11}

The kinetic parameters were determined by EIS approaches. The Nyquist plots were fitted using the equivalent circuit model. The high and low frequency semicircles are attributed to surface film resistance (R_{sf}) and charge transfer resistance (R_{ct}) at the electrode/electrolyte interface, respectively. The Li-ion diffusion coefficient (D_{Li}) from the relation between the real impedance and the angular frequency in the low frequency region were further estimated to quantitatively evaluate the S^{2-} substitution effects.

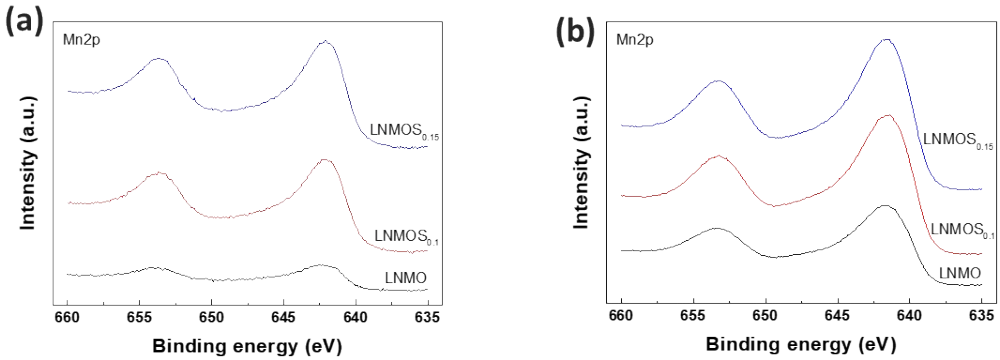

Fig. S8. Mn2p XPS core-level spectra of the 200 cycled LNMO and $LNMOS_x$ electrodes taken from (a) as prepared surface, and (b) following Ar sputtered surface.